Ground displacements around the fault of the September 20th, 1999, Chi-chi Taiwan earthquake

T. C. Shin[1], F. T. Wu[2], J. K. Chung[1], R. Y. Chen[1], Y.M. Wu[1], C.S. Chang[1], T.L. Teng[3]

Abstract. Ground displacements in the meizoseismal area of the September 20, 1999, Chi-chi earthquake are derived from accelerograms at 39 stations. On the hanging wall side a maximum horizontal, NW-directed motion of 8 meters and a vertical rise of 3.7 meters are found near the northern end of the N-S trending surface trace of the fault. On the footwall side and next to the fault a maximum horizontal motion of 1.3 meters and a maximum downward vertical motion of 1 meter are observed. The displacement field describes the source as a thrust fault with left-lateral motion. The displacements increase from south to north along the fault, and so does the left-lateral component of the fault motion, from about 10% to 60% of the total horizontal displacement. The recorded motions, especially ground velocities and accelerations, are noticeably stronger on the hanging wall side than on the footwall side.

1. Introduction

The September 20, 1999, Taiwan earthquake occurred near the town of Chi-Chi in the west-central part of the island (Fig. 1). It was a disastrous event and is the largest known earthquake on the island. The causative fault, the Chelungpu fault (Fig. 1), is essentially the western bounding fault of the mountains. This generally east-dipping fault was recognized as active in the recently published active fault map (Chang et. al., 1998), however it was presumed to have been inactive in the last 100,000 years, based on an estimated age of alluvium under the tip of the thrust. Certainly no historical damaging earthquake was known to have occurred on the fault since the mid-1600 when earthquake record keeping began. The length of the surface trace is about 77 km, striking N-S along most of its length and turning E-W at its northern end. The surface faulting associated with this earthquake is very prominent, and the damages from the mainshock were the heaviest on the hanging wall side and near the fault. Along its length the relative displacement of the two sides increases from the south toward the north. While near the southern end the motion appears to be pure thrust, strike-slip displacement becomes dominant along the N-S striking portion of the fault toward the north. After the fault turns E-W vertical offsets of

a few meters were frequently observed, whether as ramps at the surface or as steps in the rivers and streams where new waterfalls were created. All the focal mechanism solutions available so far indicate a nearly pure thrust (Harvard CMT, USGS CMT). But the left-lateral motion on the fault, especially toward the northern end, was unmistakable.

An extensive instrumentation program in the Central Weather Bureau (CWB) began in 1990 and was in place when this event occurred. The telemetered network of 73 seismic stations, equipped with velocity sensors and accelerometers, are used for routine earthquake location and also for rapid earthquake reporting. Usually within 2 minutes of the origin time the hypocentral information, accompanied by peak accelerations at the stations and an intensity map, is sent by E-mail or fax to agencies involved in emergency services and the research community. The collapse of power transmission towers in the meizoseismal area in the early seconds of the earthquake led to power outage in northern Taiwan and data from many seismic stations were missing because of it. But sufficient data from 13 stations, including 3 in northern Taiwan, were received and were used for rapid reporting.

In addition to the telemetered network, the Taiwan Strong Motion Instrumentation Program (TSMIP) of CWB operates 637 free-field accelerograph stations. Data from a subset of these stations are used for this study. In the design of TSMIP one of the requirements was the broad frequency response (from DC to 50 Hz) of the accelerometers. As a consequence, the absolute displacements around the fault can be obtained by integrating the accelerograms. For stations near the surface trace of the fault where the fault dislocation were observed directly, the displacements derived from double integration of accelerograms could be readily checked against the ground truth. Besides providing absolute coseismic displacement measurements in the region, complementing measurements based on GPS and leveling, our results also show the detailed dynamic changes in displacement field during the earthquake.

2. Data and data processing

Several types of accelerographs are used in the TSMIP but all have similar characteristics and were extensively tested (Teng et. al., 1994). A large number of the instruments are equipped with GPS clocks. Absolute time was lost however, as CWB just began to correct the "Week Number 1024 Roll Over" problem (the week number was reset to zero on August 22, 1999) when the earthquake struck. Although the absolute timing may eventually be recovered, it has not yet been done and is not needed for the current study.

In our data processing, we assumed that accelerations were zero before the arrival of P wave and thus we removed the DC level in the pre-event data. But as shown in Fig. 2a, even after this removal, the result of integrating the accelerogram is still dominated by a prominent trend, starting after many

---
[1]T. C. Shin, J. K. Chung, R. Y. Chen, Y.M. Wu, C.S. Chang, Central Weather Bureau, Taipei, Taiwan
[2]F. T. Wu, State University of New York, Binghamton, New York (e-mail: wu@sunquakes.geol.binghamton.edu)
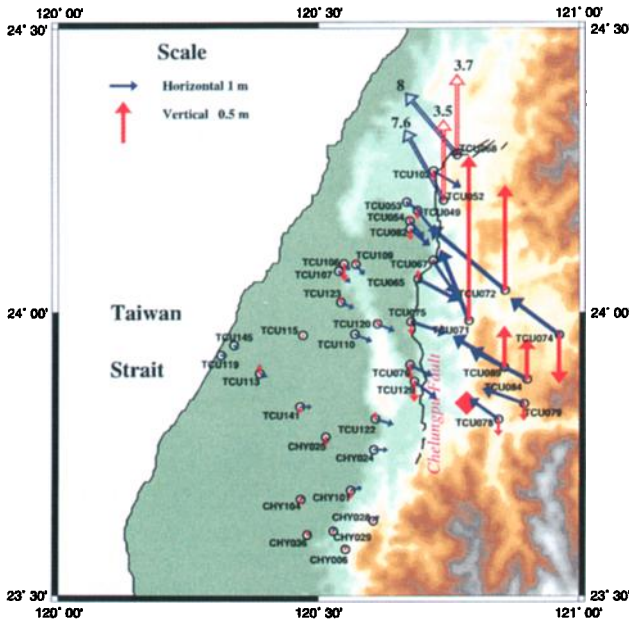[3]T.L. Teng, USC, Los Angeles, California

Figure 1. Meizoseismal area of the September 20, 1999, Chi-Chi, Taiwan, earthquake. Circles are the TSMIP stations with their names beside each circle. The blue arrows show the directions and amplitudes of the horizontal displacements at the stations. The lengths of the red arrows show the amplitudes of vertical displacements. The numbers near the tips of the arrowheads indicate the amplitudes of the unfilled arrows.

seconds of strong ground motion. Such a trend in the velocity corresponds to a DC shift in acceleration and should not be present unless mechanical hysteresis existed or the instrument had been tilted. Iwan (1985) studied a similar phenomenon. In the extensive shaking-table tests of the TSMIP instruments,
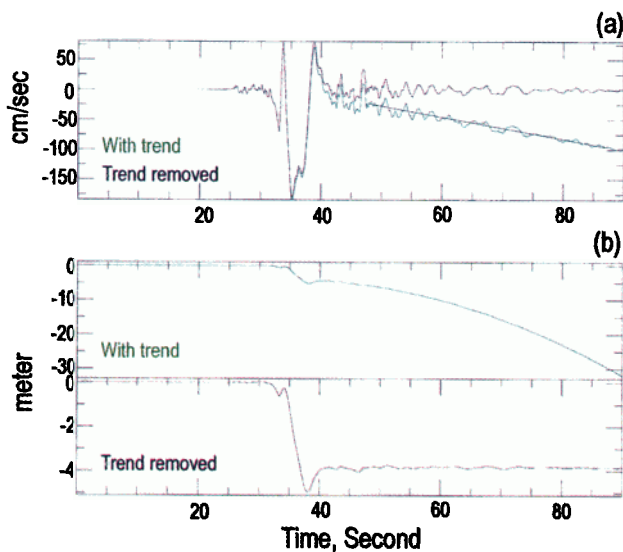

Figure 2. (a) Ground velocity obtained from integrating the E-W accelerogram at TCU052. The result of direct integration is shown in green; note the linearly growing tail and the fitted least square line. For the blue trace the trend has been removed. (b) Top: derived displacement with trend included; Bottom: displacement with trend removed.
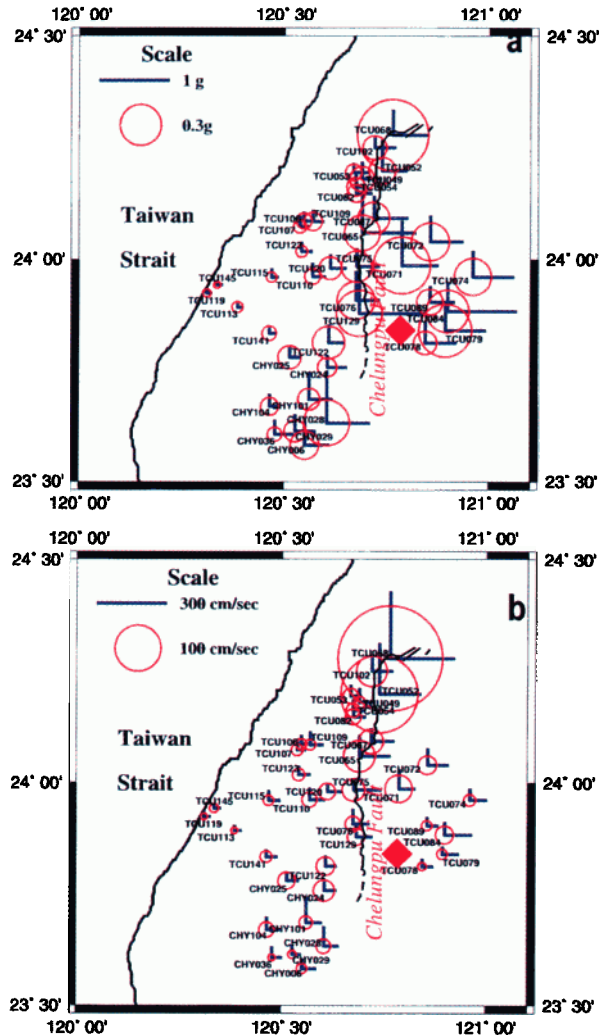

Figure 3. (a) The amplitudes of the three components ground accelerations. The lengths of the E-W and N-S lines and the radii of the circles represent the amplitudes of the E-W, N-S and vertical accelerations. The ends of the lines at each station would fall on the circle if they were all equal. (b) The corresponding amplitudes of the three components ground velocities at the same stations. The amplitudes are expressed in the same way as in (a).
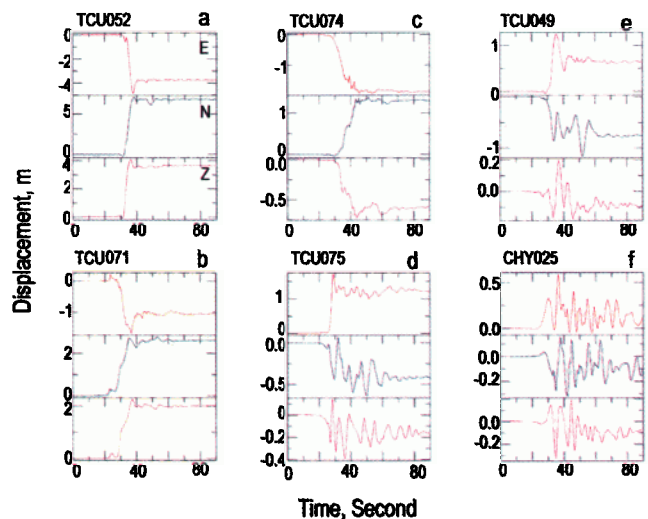

Figure 4. Example of ground displacement time series. See text.

including those with box function input, such shift did not occur (Teng et al., 1994). In the box-function tests the total displacement was 1.25 centimeters and the rise-time was about 40 millisecond, resulting in a velocity of nearly 40 cm/sec, in the range of observed values when DC shifts in data become obvious. Ground tilt could have occurred in the meizoseismal zone. Indeed, sample checking in the field uncovered instrumental disorientation at sites where large displacement had taken place. Gravitational attraction will then contribute to a shift of the acceleration level. By removing the linear trend in velocity, equivalent to removing the DC in acceleration, the effect of tilting is removed. Not removing the trend yields a displacement with a growing tail (Fig. 2b, top). With trend removal the displacement coasts to its resting position (Fig. 2b, bottom). The computed tilt angles from the trends are less than a few degrees.

When tilting has occurred, ground displacement can be accurately determined from an accelerogram only if tilt is recorded simultaneously at the site. In any case uncertainty in tilt, an insufficient record length for trend estimation and the oscillatory nature of the time series limit our ability to resolve DC displacement smaller than about ±0.1 m.

3. Displacements in the meiszoseismal area

Figure 1 shows the amplitudes and directions of horizontal and vertical displacements at stations from which we have acceleration data. The peak accelerations and velocities are shown in Fig. 3a and 3b. Although the peak accelerations are generally larger on the hanging wall side, of the two sites where E-W accelerations exceeded 1g TCU129 is on the footwall side and TCU084 on the hanging wall side. Furthermore, relatively high peak accelerations are also seen to the southwest of the fault, quite far from the fault trace and the epicenter. It is clear when comparing Figs. 3a and 3b that the stations with higher accelerations are not necessarily the stations with larger ground velocities, or displacements (see Figs. 1 and 3), implying the high frequency nature of the peak accelerations. We also note that the vertical accelerations are nearly always smaller that the horizontal components.

Several important features in the displacement field can be discerned in Fig. 1. That the ground motions on the hanging wall side are much larger than on the footwall side and generally opposite in directions is very clear. The largest ground motion is found at the northern extreme of the Chelungpu fault. There the northwest-directed horizontal displacement reaches 8 meters and the vertical displacement 3.7 meters. The displacements are generally larger toward the north and the directions of the horizontal displacement also undergo a systematic change, from nearly east west to northwesterly. Although the vertical displacements are all downward on the footwall side, those on the hanging wall side clearly change signs. Looking across the middle section of the fault, the motions are upward within about 20 kilometers of the fault and downward beyond (at stations TCU074 and TCU079). Our data agree well with the before-and-after GPS measurements (Yu et al., 1999, and Rau, 1999, personal communications) and with the dislocations observed in the field. This pattern of vertical displacement is consistent with the theoretical co-seismic deformation of a thrust fault (Savage, 1983), and we shall discuss it more later.

In general the large displacement at each station begins to build up with the arrival of the S-wave, but the waveforms vary according to the station location with respect to the fault

and perhaps the epicenter. Figs. 4a-f show six representative examples. At TCU052, very close to the northern section of the fault, on the hanging wall side, the displacement time series are essentially ramp functions with a rise time of about 5 seconds (Fig. 4a). The displacements farther east on the hanging wall side (at TCU071) are still ramps and the horizontal displacement vector is in the same direction as at TCU052. The rise times however are longer, about 10 seconds, and the amplitudes of displacements are much smaller (Fig. 4b). Further toward the east, the horizontal motions are in the same directions as those of the last two stations are but the vertical motion is down instead of up as seen at TCU074 (Fig. 4c). Very close to the fault, but on the footwall side, the rise time of the E-W component is still fairly short, around 5 seconds, but the N-S and vertical motions are more oscillatory and approaches the final displacements more gradually, as shown at station TCU075 (Fig. 4d). The combined horizontal displacement is 1 meter and the vertical motion is less than 0.2 meters. For stations farther away from the fault and on the footwall side the horizontal DC offsets are less than 1 m and the vertical offset on the order of 0.1-0.2 m (TCU049, Fig. 4e). For stations located in the plain to the west of the fault, the displacement becomes oscillatory with DC offsets in the 0.1-0.2 meters range (Fig. 4f). The stations where the displacement seismograms show similarity to those illustrated, as identified by letters "a"-"f", are listed in Table 1. Incidentally, discernible long period displacements after P arrivals are sometimes seen, e.g., on the N-S and vertical components at TUC071 (Fig. 4b), perhaps a result of near-field radiation (Aki and Richards, 1980).

4. Discussion

The establishment of TSMIP in the mid-1990's allowed the capture of the ground motions around the source zone of the $M_w=7.6$ Chi-chi earthquake. The recorded maximum peak acceleration exceeds 1g and the ground velocity more than 290 cm/sec, some of the largest values ever seen in an earthquake. The combination of large ground motion and adequate DC instrument response made it possible to investigate ground displacement around the fault in some detail. Judging from the displacement data obtained so far, this earthquake has several peculiar characteristics. As shown by the displacement vectors in Fig. 1, and also by the surface rupture, the earthquake fault is a pure thrust at the southern end and becomes a thrust with a large left-lateral strike-slip component toward the north. This is in contrast to all known first motion and CMT solutions (Harvard CMT, USGS CMT, ERI, CWB, etc., 1999). For solutions based on body waves,

Table 1. Types of Displacement Seismograms
FW=footwall; HW=hangingwall

Type	Location	Stations with similar waveforms
a	Near fault-HW	(TCU)052,068
b	Mid-East-HW	(CHY)072,071,084,089
c	Far East-HW	(TCU)078,079,074
d	Near fault-FW	(TCU)065,067,075,076,102,129
e	Near West-FW	(TCU)049,053,054,082,110,112, 115,120,122
f	Far West-FW	(TCU) 107, 109,119,123,141,145

with dominant wavelengths as short as a few kilometers, this dichotomy can perhaps be readily understood as a result of modeling mainly the early part of the waveform. But for solutions based on broadband seismograms and especially those on long period surface waves (Harvard CMT), this contradiction cannot be easily explained. The true nature of faulting and its relation to focal mechanisms based on teleseismic seismic waves can perhaps be resolved when modeling includes the near source displacements.

The relative amplitudes of displacements on the hanging wall and the footwall sides are quite striking. This difference between the ground motions on two sides of a thrust fault has been found in physical or numerical modeling and in strong motion records (Shi et al., 1998; Huang and Yeh, 1994; Oglesby et al., 1998), but it has never been so clearly shown. It is perhaps not surprising this should occur, since the motion of the hanging wall is essentially free while the footwall has to advance against the deeper crustal material in its front. The vertical displacements on the footwall side all point downward can also be expected, but it is interesting to note the differences between the displacement time functions on two sides of the fault even when they are very close. For example, on the hanging wall side at TCU052 the ground comes to rest essentially after 6 or 7 seconds after the beginning of the strong ground motion, but on the footwall side at TCU075, the motion continues for 20 seconds in N-S and the vertical directions (Fig. 4d). The subsidence of the footwall side is evidently a long-term process, consonant with the presence of a major sedimentary basin under the frontal part of the fault.

The vertical displacement field on the hanging wall side is interesting when considering the vigorous mountain building activity in Taiwan (Wu et. al., 1997). As we saw earlier, subsidence occurs about 20 km east of the fault where mountains begin to rise (e.g., station TCU074 in Fig.1) and even at shorter distances toward the south (TCU078 in Fig. 1). Similar co-seismic uplift and subsidence from thrust faulting has been observed and modeled in subduction zones (e.g., Savage, 1983; Savage, 1998). Savage noted (1983) that long-term subduction does not lead to the cumulative deformation of the overthrust plate in the subduction environment. But in the present case, evidently the uplift of the mountain range in between the earthquake episodes is substantial (Yu and Kuo, 1999). At a rate of ~10 mm/yr in the higher ranges, the rise is enough to offset the subsidence during the earthquakes and the effects of denudation. The long-term bending and shortening of the Taiwan crust that caused the uplift also led to episodic crustal rebounds. Chi-Chi earthquake is one of the rebound events, not dissimilar to that in the Rebound Theory (Reid, 1906) for strike-slip fault. In Taiwan the mountain building results mainly from the non-elastic interseismic uplifting. The subsidence at TCU078 and TCU079, however, could very well be the result of tension developed due to the overall northward motion of the hanging wall block.

5. Conclusion

The September 20, 1999, Chi-chi earthquake is a well-instrumented major event. The island-wide accelerograph network deployed in the mid-1990's captured the strong motion records at more than 300 sites at the end of October. The ground velocities and displacements obtained from accelerograms produced some of the largest values ever observed. The displacements agree well with surface breaks observed near the fault trace and also with GPS results measured at nearby sites in both amplitude and direction. However our data provides the time history of the displacements during the dynamic stage of the fault growth. Also our data contain the co-seismic part only while GPS may include pre- and post-seismic components.

Displacements both near the surface break and in the area around it show that the fault is mainly an oblique thrust with ground motions on the hanging wall side much greater than those on the footwall side.

References

Aki, K., and P.G. Richards, 1980. Quantitative Seismology. Vol. 1. Freeman and Company, San Francisco, 557p.
Chang, H.C., C.W. Lin, M.M. Chen, and S.T. Lu. , 1998. An introduction to the active faults of Taiwan: Explanatory text of the active fault map, Central Geological Survey, MOEA, Taiwan, 103pp. (In Chinese)
Huang, B.S. and Y.T. Yeh, 1994. Ground motion of a propagating rupture fault from the finite element modeling, TAO, v. 5, 295-321.
Iwan, W.D., M.A. Moser, C.Y.Peng, 1985. Some observations on strong-motion earthquake measurement using a digital accelerograph, Bull. Seism. Soc. Am., v. 75, 1225-1246.
Oglesby, D., R.J. Archuleta, and S.B. Nielsen, 1998. Earthquakes on dipping faults: The effects of broken symmetry, Science, v. 280, 1055-1059.
Reid, H.F., 1910. The mechanics of the earthquake. In Lawson, A.C., chmn., he California Earthquake of April 18, 1906. Carnegie Institute of Washington Publication 87, v.2, 192p.
Shi, B.P., A. Anooshehpoor, J.N. Brune, and Y.H. Zeng, 1998. Dynamics of thrust faulting: 2-D lattice model, Bull. Seism. Soc. Am., v. 88, 1484-1494.
Savage, J.C., 1983. A dislocation model of strain accumulation and release at a subduction zone, Jour. Geophys. Res., v. 88., 4984-4996.
Savage, J.C., J.L. Svarc, W.H. Prescott, W.K., 1998. Deforamation across the rupture zone of the 1964 Alaska earthquake, 1993-1997.
Teng, T.L., M. Hsu, W.H.K. Lee, Y.B. Tsai, F.T. Wu, Y.T. Yeh and G. Liu, 1994. Instrumentation Evaluation and Strong-motion Software Development, Annual Report to Central Weather Bureau, 104pp.
Wu, F. T., R. J. Rau, and D. H. Salzberg, Taiwan tectonics: thin-skinned or lithospheric collision, Tecotnophysics, v. 274, 191-220, 1997.
Yu, S.B., and L. C. Kuo, 1999. Three dimensional crustal deformation in the arc-continent collision zone of southern Taiwan, Memoirs Geosciences-Montpellier, No. 14, p. 79, University of Montpellier.